Fusion Engineering and Design 197 (2023) 114055

Contents lists available at ScienceDirect

Fusion Engineering and Design

journal homepage: www.elsevier.com/locate/fusengdes

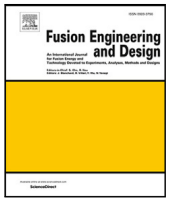

ADRANOS: A numerical tool developed to analyse coolant operating conditions of the EU-DEMO divertor

A. Quartararo *, P.A. Di Maio, E. Vallone

Department of Engineering, University of Palermo, Viale delle Scienze, Ed. 6, 90128 Palermo, Italy

ARTICLE INFO

Keywords:
EU-DEMO
Divertor
Plasma facing components
Thermofluid-dynamics
Monoblock

ABSTRACT

In the context of the activities of the EUROfusion action, the University of Palermo has carried out a research campaign to evaluate the thermal-hydraulic performance of the EU-DEMO divertor Single-Circuit Cooling (SCC) option. Given the exceptional geometric complexity of this divertor design, the search for coolant operating conditions that comply with the applicable design constraints cannot be performed by relying on detailed 3D computational fluid-dynamic calculations. For this purpose, the Advanced Divertor paRametric Analysis for coolaNt Operating Scenarios (ADRANOS) code has been developed. It is a novel numerical tool capable of quickly assessing the thermofluid-dynamic behaviour of the divertor cooling circuit with reduced computational cost, predicting the divertor performance map at different coolant inlet conditions and mass flow rates, and allowing for the effortless study of different circuit topologies.

This study introduces the ADRANOS modelling approach, describes its validation process, and demonstrates its application to various configurations of the SCC divertor option. The results obtained showed that it is possible to find suitable coolant operating conditions characterized by low temperature and high pressure, posing a challenge for the adoption of Eurofer as a structural material.

1. Introduction

One of the main challenges in the realization of a fusion reactor able to deliver electricity to the grid, such as the EU-DEMO, is the control of power exhaust, as emphasized by Mission 2 of the European Research Roadmap to the Realisation of Fusion Energy [1].

The divertor is a critical in-vessel component in this context. Its main functions are to continuously remove the power deposited by charged particle bombardment and neutron irradiation, provide gas streaming channels towards the pumping ports to exhaust helium and unburnt fuel, be equipped with plasma-facing surfaces physically compatible with the plasma, and shield the vacuum vessel and magnets from nuclear loads [2]. The divertor must be designed to perform its functions according to certain engineering requirements, i.e. to reduce nuclear waste, to minimize costs and maximize the material recycling potential, and finally to minimize the design complexity with the aim to reduce the maintenance downtime [3].

The baseline EU-DEMO divertor consists of 48 toroidally-arranged cassette modules [4]. Each cassette, as depicted in Fig. 1, comprises several sub-components: two Vertical Targets (VTs), a Shielding Liner (SL), two Reflector Plates (RPs) and a Cassette Body (CB) supporting all the other sub-components.

The EU-DEMO divertor baseline is based on the Double-Circuit Cooling (DCC) option concept, as it foresees two cooling circuits [2], one for the VTs and one for the CB and the remaining sub-components, this latter simply referred to as CB cooling circuit. Sub-cooled pressurized water is employed as a coolant for both the cooling circuits, and, due to the specific thermal loads expected on the different parts of the divertor, different coolant operating conditions are required. Therefore, the baseline EU-DEMO divertor design foresees two independent Primary Heat Transfer Systems (PHTSs).

Although the Gate Review carried out at the end of the EU-DEMO Pre-Concept Design phase [5] endorsed the divertor baseline design and selected technologies, it was suggested to investigate a Single-Circuit Cooling (SCC) option cassette to simplify the balance of plant design with a single PHTS, and to ease remote maintenance with two pipes (inlet/ outlet) instead of four to be cut and rewelded.

In the frame of EUROfusion development activities, the University of Palermo (UNIPA) thermal-hydraulic research team has developed a calculation tool dedicated to studying the thermofluid-dynamic behaviour of the divertor cooling circuit. This novel tool, named Advanced Divertor paRametric Analysis for coolaNt Operating Scenarios (ADRANOS), has been conceived to predict, with a reduced computational effort, the thermal-hydraulic performance map of the divertor.

* Corresponding author.
E-mail address: andrea.quartararo@unipa.it (A. Quartararo).

https://doi.org/10.1016/j.fusengdes.2023.114055
Received 28 July 2023; Received in revised form 25 October 2023; Accepted 29 October 2023
Available online 6 November 2023

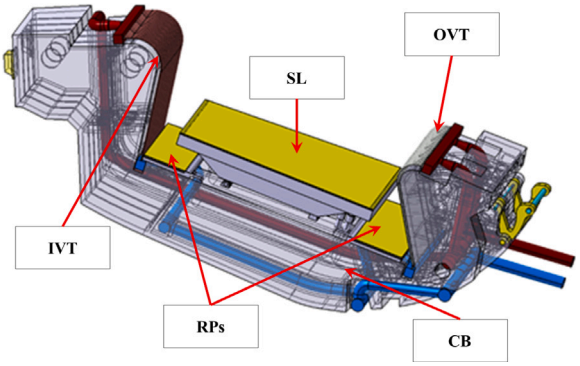

Fig. 1. EU-DEMO divertor cassette (DCC option).

Table 1
Nominal heat fluxes prescribed for the EU-DEMO divertor [2].

Heat fluxes	Value
Maximum heat flux on VTs during normal operation	≈10 MW/m^2
Maximum heat flux on VTs during slow transient events	≈20 MW/m^2
Maximum heat flux on SL during normal operation	≈1 MW/m^2
Maximum heat flux on RPs during normal operation	≈0.2 MW/m^2

The aim is to find suitable coolant operating conditions to be adopted for the SCC divertor option and to highlight possible criticalities of this concept.

2. The EU-DEMO divertor cooling circuits

The divertor cooling circuits are designed to remove the specified surface and volumetric heat loads during normal and off-normal operations, to ensure that structural and functional materials operate within their optimal temperature ranges to safely guarantee the envisaged divertor lifetime.

The nominal surface heat loads of the EU-DEMO divertor are reported in Table 1; the maximum volumetric heat loads of the cassette is around 12 MW/m^3 [6]. With reference to Table 1, the slow transient events are plasma transients characterized by increased thermal loads on the divertor VTs, whose duration is in the order of 10 s of seconds, long enough to reach the thermal equilibrium in the monoblocks [2].

As it may be argued from the table, there is an order of magnitude of difference between the surface loads foreseen on the VTs and those of the other divertor sub-components. This difference is the motivation for the selection of separate cooling circuits for the baseline EU-DEMO divertor, as will be detailed in the following section.

2.1. Divertor double-circuit cooling option

The VTs cooling circuit has been conceived to withstand the outstanding heat fluxes reported in Table 1 [7], which are concentrated within a narrow band (the poloidal extension of the loaded region is approximately ±50 mm around the strike point [2]), resulting in a peaked power distribution. The VTs cooling requires high mass flow rates of low-temperature water, resulting in average velocities inside the cooling channels, in the range of 12–15 m/s [8]. These coolant operating conditions are necessary to guarantee a sufficient safety margin against the Critical Heat Flux (CHF) occurrence under 20 MW/m^2 surface heat load conditions, in order to avoid dry-out phenomena that could jeopardize the target structural integrity.

The DCC VTs cooling circuit foresees the two VTs connected in parallel. These are composed of a toroidal array of 31 and 43 Plasma Facing Unit (PFU) assemblies, respectively for the Inner VT (IVT) and the Outer VT (OVT) [9]. The pipes and distributors/manifolds of the VTs cooling circuit are made of AISI 316 [10]. Each PFU assembly consists of a long cooling pipe made of CuCrZr equipped with a Swirl Tape (ST) turbulence promoter, armoured with a longitudinal array of tungsten monoblocks joined to the pipe with a thin copper interlayer. An exploded view of a PFU assembly foreseen for the EU-DEMO divertor is shown in Fig. 2.

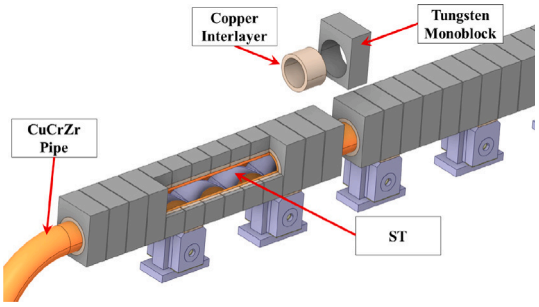

Fig. 2. Exploded view of a divertor PFU assembly.

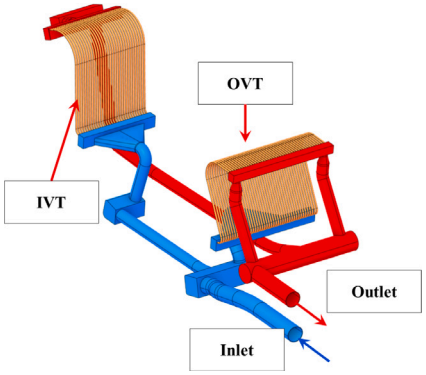

Fig. 3. EU-DEMO divertor VTs cooling circuit (DCC option, 2019 design).

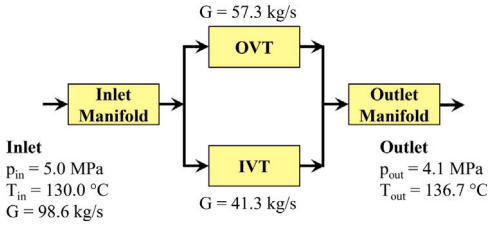

Fig. 4. EU-DEMO divertor VTs cooling circuit scheme (DCC option, 2019 design).

The DCC VTs cooling circuit is depicted in Fig. 3, and its schematic flowchart in Fig. 4 together with the temperatures, pressures, and mass flow rates calculated in [8].

The CB cooling circuit is devoted to the cooling of the other divertor sub-components, i.e. CB, SL, and RPs. These components are made of Eurofer and both SL and RPs are coated with a thin layer of tungsten on surfaces directly exposed to the plasma. The layout of the cooling circuit is shown in Fig. 5, while its cooling scheme is visible in Fig. 6 with an indication of temperatures, pressures, and mass flow rates [11].

As can be noted from Fig. 6, the CB cooling circuit is supplied with cooling water at a higher temperature compared to the VTs, while both mass flow rate and pressure are lower. The higher coolant temperature is allowed by the significantly lower thermal loads expected for the CB, SL, and RPs (Table 1) and is necessary to adopt Eurofer as structural material.

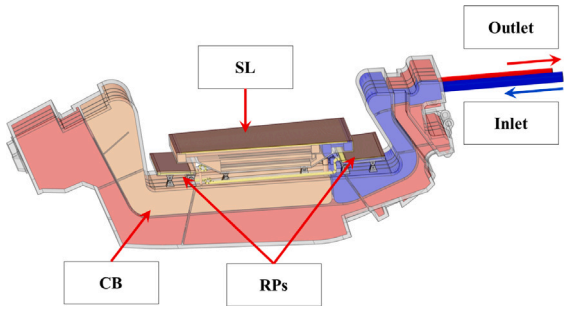

Fig. 5. EU-DEMO divertor CB cooling circuit (DCC option, 2019 design).

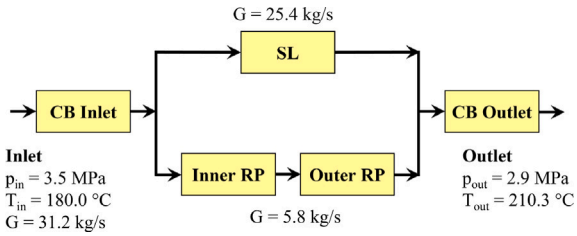

Fig. 6. EU-DEMO divertor CB cooling circuit scheme (DCC option, 2019 design).

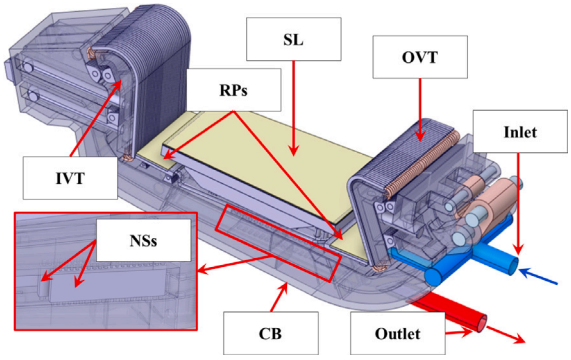

Fig. 7. EU-DEMO divertor cassette (SCC option, 2021 design).

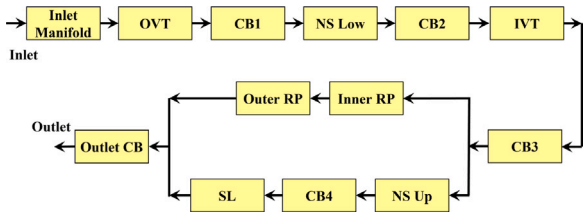

Fig. 8. EU-DEMO divertor cooling circuit scheme (SCC option, 2021 design).

2.2. Divertor single-circuit cooling option

The SCC option divertor was developed for EU-DEMO in 2021 [12] (Fig. 7). Similarly to the DCC option, the cassette is made of Eurofer and is equipped with two VTs, one SL, two RPs, and additionally a pair of Neutron Shields (NSs) to improve neutron shielding in the vacuum pumping hole. The cooling scheme of the SCC option divertor is shown in Fig. 8.

The coolant mass flow rate and inlet operating conditions to be adopted for the EU-DEMO divertor SCC option must comply with the requirements of both the VTs and the Eurofer sub-components of the cassette, and are yet to be selected.

A 3D Computational Fluid-Dynamic (CFD) simulation of the SCC divertor has been performed in [6], tentatively considering cooling water at 130 °C and 7.0 MPa and with the highest coolant mass flow rate allowed to stay within the maximum pressure drop limits. Under these operating conditions, insufficient CHF margins for the VTs have been observed.

However, different coolant operating conditions or cooling circuit layouts of the SCC option could be able to guarantee the compliance with several design constraints and requirements for the divertor, which are detailed in the following section.

3. Thermal and thermo-hydraulic constraints

The design of the EU-DEMO divertor cooling circuits has been driven by the following set of thermal-hydraulic design constraints, drawn from [9].

1. Maximum water axial velocity in PFU cooling channels lower than 16 m/s;
2. water total pressure drop for each cooling circuit lower than 1.4 MPa;
3. CHF margin of VTs higher than 1.4 under the nominal heat flux of 20 MW/m^2;
4. CHF margin of SL and RPs higher than 1.4 under the nominal heat fluxes of respectively 1 and 0.2 MW/m^2;
5. minimum margin against saturation temperature higher than 20 °C;
6. structural and functional materials operation within the acceptable temperature range.

Concerning the CHF margin M_{CHF}, it is defined as the ratio between the *incident* CHF, as given in [13], and the heat flux on the plasma-facing walls.

For the DCC option divertor, constraints 1, 2, 3, and 6 apply to the VTs cooling circuit, while 2, 4, 5, and 6 to the CB cooling circuit. The SCC option has to be designed to meet all the above-mentioned constraints. In particular, the maximum pressure drop limit of 1.4 MPa has not been increased, even if the SCC option 2021 design foresees the VTs connected in series to each other and to the cassette.

The compliance with most of the constraints listed above can be verified based on rather simple calculations by applying the First Principle of Thermodynamics and adopting appropriate correlations, for example following the procedure described in [14].

Concerning the structural and functional materials' temperatures, the verification of temperature constraints must be performed by adopting complex 3D coupled (fluid–structure) thermofluid-dynamics calculations due to the geometrical complexity of the divertor. Nevertheless, it is possible to determine the maximum temperatures reached within the PFUs, which are critical components from a thermal standpoint, using simple steady-state 2D calculations. It is feasible due to their relatively simple geometry, the peaked shape of the surface power density, and the low thermal inertia of these components, which reach stationary conditions within a few tens of seconds, as can be argued from [15].

In this work, the following set of constraints on acceptable temperatures relevant to the PFU materials is considered, in accordance with [16]:

- maximum tungsten temperature lower than 3222 °C (200 °C margin against melting);
- maximum copper interlayer temperature lower than 885 °C (200 °C margin against melting);
- maximum allowable CuCrZr pipe temperature below 300 °C at 10 MW/m^2 (to be calculated as average over the pipe thickness) to guarantee negligible creep;

- maximum allowable CuCrZr pipe temperature below 450 °C at 20 MW/m^2 (to be calculated as average over the pipe thickness) to guarantee negligible creep.

This list of temperature constraints is not meant to be exhaustive, but can be verified very easily and allows for an initial screening of unsuitable divertor coolant operating conditions.

Concerning the other divertor materials, particular attention must be paid to the Eurofer temperature. Although the optimal operating temperature range for this material is 350-550 °C [2], the design of the divertor cassette has been carried out over the last years considering a Eurofer minimum operating temperature of 180 °C, according to the rationale described in [17]. Operating the divertor at these low temperatures implies a strong constraint on the maximum irradiation damage dose, finally resulting in a lower component lifetime. The most critical component of the baseline DCC cassette is the SL, whose expected lifetime is 1.2 Full Power Year (fpy), lower than the target value of 1.5 fpy [2]. Moreover, according to what is reported in [17], the cassette lifetime increases with its coolant operating temperature. It is not possible to check whether the Eurofer temperature exceeds the 550 °C upper limit with simple numerical tool. However, the minimum temperature in Eurofer can be reasonably assumed equal to the coolant inlet temperature and, therefore, it is possible to provide an indication of the divertor lifetime.

4. ADRANOS development

4.1. Overview

ADRANOS is a coupled lumped-parameter/2D Finite Element Method (FEM) simulation tool created with the aim of assessing the steady-state performance map of the EU-DEMO divertor cooling circuit, to be intended as the domain of the phase space of coolant inlet mass flow rate, pressure and temperature conditions that allow the cooling system to safely carry out its target mission in compliance with the constraints discussed in the previous paragraph.

The code has been developed in MATLAB® [18] with an object-oriented approach, to make it highly flexible in evaluating different cooling system topologies. Moreover, it has been optimized for parallel computing to greatly reduce the overall time required to perform the simulations.

The code takes advantage of the FEA toolbox [19] FEM solver available in the MATLAB® package, employed to perform 2D steady-state thermal analyses of the PFU monoblocks located at the IVT and OVT strike points, to evaluate the temperature distribution in the most critical region of the VTs.

The methodologies and procedures implemented in ADRANOS are based on the codes developed in [20–23]. With respect to these codes, ADRANOS has been purposely developed with the aim of evaluating the performance map of the divertor. Therefore, the code is optimized to carry out quickly and automatically thousands of simulations, considering different coolant operating conditions. It is possible because the code allows for parallel computing, the FEM and lumped parameters simulations are performed within a single coding environment thus allowing the straightforward coupling between the two modules, and the code outcomes are collected and post-processed automatically.

The modelling approach of ADRANOS is thoroughly described in the following sections. SI units are used for all equations herewith presented unless explicitly stated.

4.2. Methodology - Lumped parameters module

The ADRANOS lumped-parameters module requires the preliminary breakdown of the cooling circuit into different volumes, which can be performed arbitrarily according to the required level of detail. In the following, one volume for each divertor sub-component (e.g. SL, inner RP, outer RP, etc.) will be considered. The volumes can be connected in series or parallel, and it is furthermore possible to group them so to ease the circuit definition, as well as to perform more detailed 1D assessments (e.g. if it is required to obtain pressure and/or temperature profiles). The layout of the input cooling circuit is provided to the code in the form of a flowchart, similar to those reported in Figs. 4, 6 and 8.

Each volume j entails being provided with the hydraulic characteristic equation $\Delta p(G)$, defined according to Eq. (1), where Δp is the total pressure drop, ρ is the average density calculated starting from the average values of temperature $\overline{T}_j$ and pressure $\overline{p}_j$ inside the volume (arithmetic averages between inlet and outlet conditions), and G is the mass flow rate.

$$\Delta p \frac{\rho_{ref,j}}{\rho\left(\overline{T}_j, \overline{p}_j\right)} \alpha_j G^{\gamma_j} \tag{1}$$

Due to the geometrical complexity of the divertor sub-components, the $\Delta p(G)$ function cannot be defined on the basis of simple correlations. Hence, the code relies on preliminary thermofluid-dynamic analyses performed with dedicated 3D-CFD calculations. More in detail, starting from the results of CFD simulations, a set of Δp values at different mass flow rates is collected for each fluid region corresponding to the jth volume of the ADRANOS discretization. Therefore, a curve with the general form $\Delta p = \alpha_j \dot{G}^{\gamma_j}$ is fitted, where α_j and γ_j are proper fitting coefficients. A density correction term $\rho_{ref,j}/\rho\left(\overline{T}_j, \overline{p}_j\right)$ is moreover considered to take into account the variations of pressure drop with the coolant temperature, following the rationale reported in [14]. The reference density $\rho_{ref,j}$ of Eq. (1) is calculated from the supporting CFD simulations as a proper volume-averaged density value.

Indeed, the adoption of supporting CFD simulations for the evaluation of pressure loss distribution among the main divertor sub-components may undoubtedly be time-consuming. However, these data are generally provided, with the same level of detail required by ADRANOS, as an output of dedicated activities carried out within the Work Package Divertor of EUROfusion. Therefore, further CFD calculations are usually not required.

Moreover, if pressure drop values are provided at a single mass flow rate, the γ_j exponent of Eq. (1) can be set equal to 2 under the assumption of turbulent flow regime, according to the rationale presented in [14].

The code solves sequentially the cooling circuit, starting from the inlet volume and proceeding downstream to the outlet of the circuit. For each volume j, for a given set of inlet conditions $T_{in,j}$, $p_{in,j}$ and a given G_j, the energy conservation equation in steady-state conditions Eq. (2) and the pressure drop equation rewritten as reported in Eq. (3) are solved iteratively. With reference to the following equations, c_p is the fluid heat capacity under isobaric conditions, calculated at the volume average values of pressure and temperature, and W_j is the total power (sum of surface and volumetric heat loads) deposited onto the volume.

All the thermodynamic and transport properties of water, such as c_p and ρ in the following Eqs. (2) and (3), are dependent on temperature and pressure and are calculated by adopting a MATLAB® implementation [24] of the IAPWS IF97 water library [25].

$$T^i_{out,j} = T_{in,j} + \frac{W_j}{G_j c_p\left(\overline{T}^{i-1}_j, \overline{p}^{i-1}_j\right)} \tag{2}$$

$$p^i_{out,j} = p_{in,j} - \frac{\rho_{ref}}{\rho\left(\overline{T}^{i-1}_j, \overline{p}^{i-1}_j\right)} \alpha_j G^{\gamma_j}_j \tag{3}$$

At each iteration i, outlet temperature and pressure values are updated considering the fluid properties obtained from the previous iteration, and the calculation proceeds until relative errors of outlet temperature and pressures calculated at two consecutive iterations result lower than a given tolerance, set equal to 0.01%.

The code is moreover capable of handling the parallel connection of two components (namely A and B) by performing an additional outer loop. In this case, an optimization algorithm is employed to find the value of the branching factor χ, defined according to Eq. (4) (where G_A the mass flow rate flowing inside the branch A), such that the difference between the pressure drops in the two branches is the same.

$$\chi = \frac{G_A}{G_A + G_B} \tag{4}$$

The factor χ is iteratively updated by adopting the Golden-section search algorithm [26], until the ratio between the pressure drop unbalance of the branches and the average pressure drop reaches values below a given tolerance, chosen equal to 0.01%. Each outer optimization iteration requires an inner loop to obtain consistent pressure and temperature values, according to Eqs. (2) and (3).

Once the iterative procedure converges, the outlet pressure (the same for the two branches) is adopted as input value for the following volume, while the temperature to be passed downstream is obtained by solving the energy conservation law for two mixing flows of Eq. (5), where h is the fluid specific enthalpy.

$$h_{out}\left(T_{out}, p_{out}\right) = \chi h_{out,A}\left(T_{out,A}, p_{out}\right) + (1-\chi)\, h_{out,B}\left(T_{out,B}, p_{out}\right) \tag{5}$$

When the average temperature and pressure values are available for all the components, the margin against saturation is assessed according to Eq. (6), where T_{sat} is the saturation temperature calculated at the outlet volume pressure. This variable is estimated and stored for each volume, and the minimum value over the entire cooling circuit is successively compared with the applicable constraint.

$$\Delta T_{sat,j} = T_{sat}\left(p_{out,j}\right) - T_{out,j} \tag{6}$$

Special attention is moreover paid to the VT volumes, which additionally requires estimating the CHF margin and maximum coolant velocity. Each VT volume must be provided with the number and geometrical details of the PFU cooling channels, i.e. the CuCrZr pipe inner diameter, the thickness and the twist ratio of the ST.

Firstly, the average coolant axial velocity along PFU cooling channels is determined according to Eq. (7), where A is the cross-section of each channel while n_j is the number of PFU cooling channels of the selected VT.

$$\overline{v}_j = \frac{G_j}{n_j A \rho\left(\overline{T}_j, \overline{p}_j\right)} \tag{7}$$

Once the axial fluid velocity is obtained, knowing the fluid average thermodynamic conditions and the geometrical details of the PFU cooling channels, the CHF margin can be derived. The well-known Tong-75 correlation of Eq. (8) is employed to calculate the CHF according to the procedure described in [13], where f_j is the Fanning friction factor, calculated according to Eq. (9), r is the enthalpy of vaporization, p_{crit} is the water critical pressure (22.064 MPa), Re_j is the Reynolds number, calculated according to Eq. (10), Ja_j is the Jacob number, calculated as per Eq. (11), and finally C_f is a factor to account for the specific geometrical configuration, that, for the case of an ST-equipped tube can be assumed equal to 1.67.

$$CHF_j = 0.23 f_j \frac{G_j}{n_j A_j} r\left(\overline{p}_j\right) C_f \left[1 + 0.00216\left(\frac{\overline{p}_j}{p_{crit}}\right)^{1.8} {Re_j}^{0.5} Ja_j\right] \tag{8}$$

$$f_j = 8 {Re_j}^{-0.6}\left(\frac{d_h}{d_0}\right)^{0.32} \tag{9}$$

$$Re_j = \frac{\overline{v}_j d_h \rho\left(\overline{T}_j, \overline{p}_j\right)}{\mu_b\left(\overline{T}_j, \overline{p}_j\right)} \tag{10}$$

$$Ja_j = \frac{\rho\left(\overline{T}_j, \overline{p}_j\right)}{\rho_{v,j}} \cdot \frac{c_p\left(T_{sat}\left(\overline{p}_j\right) - \overline{T}_j\right)}{r\left(\overline{p}_j\right)} \tag{11}$$

The Tong-75 correlation is valid for a coolant pressure between 6.9 and 13.8 MPa [27], but it is successfully employed in [28] outside this pressure range, maintaining good agreement with experimental data.

Moreover, with reference to equations Eqs. (8)–(11), d_h is the PFU cooling channel hydraulic diameter that can be calculated with Eq. (12), where d_i is the pipe inner diameter and δ is the ST thickness, d_0 is a reference diameter equal to 12.7 mm, μ_b is the water bulk dynamic viscosity, and ρ_v is the water vapour saturation density calculated at the fluid pressure. Furthermore, the average block pressure $\overline{p}_j$ is calculated net of the fluid dynamic pressure $\frac{1}{2}\rho\left(\overline{T}_j, \overline{p}_j\right)\overline{v}_j^2$, and the calculation of the CHF is made assuming that at the strike point the coolant is at the average water thermodynamic conditions within the VT volume.

$$d_h = \frac{\pi d_i - 4\delta}{\pi + 2 - 2\delta/d_i} \tag{12}$$

Once the CHF is calculated, it is compared with the maximum heat flux $q_{w,max}$ expected at the interface between the PFU cooling channel and the coolant. It is obtained by multiplying the 20 MW/m^2 nominal heat flux onto the armour plasma-facing surface by a peaking factor (equal to 1.60 for the considered monoblock geometry), required to take into account the uneven distribution of the heat flux around the pipe diameter. The CHF margin M_{CHF} definition is given in Eq. (13), where the factor 0.95 is employed to take into account the uneven flow distribution among the PFU cooling channels. In particular, a 5% deviation from average CHF value is considered, conservatively taken on the basis of the past 3D-CFD calculation results of the entire EU-DEMO divertor VTs cooling circuit [6,8].

$$M_{CHF,j} = 0.95 \frac{CHF_j}{q_{w,max}} \tag{13}$$

Similarly, the maximum velocity in the PFU cooling channels is calculated for each target by increasing the average velocity of Eq. (7) of 5%, again in accordance with the results of past 3D-CFD simulations [6, 8].

ADRANOS, once supplied with the range and the number of sample points to be considered for inlet pressure, inlet temperature and mass flow rate, performs all the calculations described above. For each triplet (p_{in}, T_{in}, G), ADRANOS checks whether the cooling circuit can provide results compatible with the constraints of maximum pressure drop, minimum saturation margin, adequate CHF margin and maximum PFU channel coolant velocities for both IVT and OVT, in accordance with the limits listed in Section 3. The CHF margin on SL and RPs is not currently calculated by the code, as it is generally much higher than 1.4 [6,11].

4.3. Methodology - 2D FEM thermal analyses module

The ADRANOS FEM module performs 2D steady-state thermal simulations of a section of the monoblock located at the strike point. The calculations are performed both for IVT and OVT and considering surface heat loads under normal operation and slow transient conditions, adopting the heat fluxes reported in Table 1.

The geometrical details of the domain considered are depicted in Fig. 9 while the mesh adopted for the 2D simulations is shown in Fig. 10 (only half domain is taken into account for symmetry). Moreover, the different regions, characterized by different materials (tungsten, CuCrZr and copper), and the nomenclature adopted for the boundaries are depicted in Fig. 10.

The computational mesh, whose details are summarized in Table 2, has been selected by preliminary performing a grid-independence study considering both 10 and 20 MW/m^2 incident heat fluxes. The mesh-independence assessment has been carried out by a generalized Richardson extrapolation procedure, as defined in [29], and the results obtained are reported here briefly. In particular, it has been observed

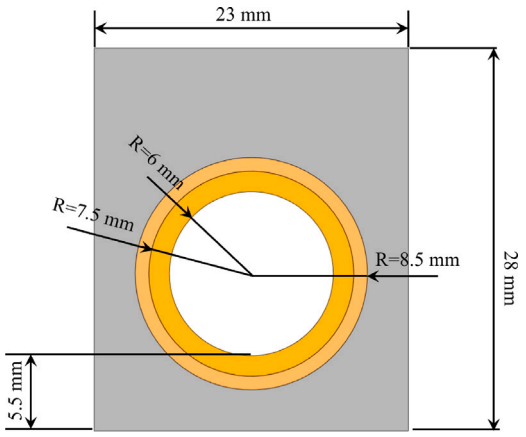

Fig. 9. Geometrical details of the EU-DEMO PFU monoblock slice.

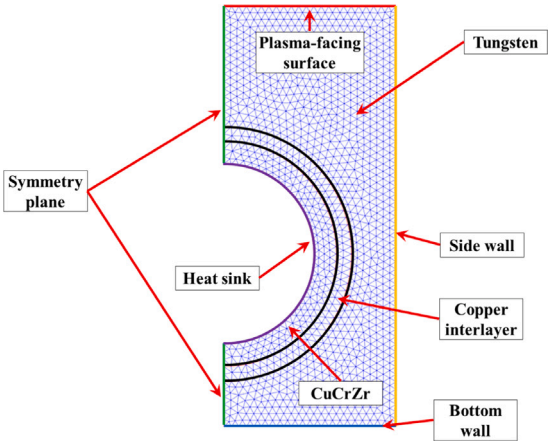

Fig. 10. Mesh adopted for the monoblock steady-state thermal simulations with indications of the regions and boundary nomenclature.

Table 2
Summary of the main mesh parameters.

Mesh parameter	Value
Nodes	1279
Elements	2384
Elements order and topology	Linear Tria
Maximum element size [mm]	0.5
Minimum element size [mm]	0.25
Mesh growth rate	1.5

Table 3
Summary of BCs adopted for the simulations.

Boundary	Applied BC
Plasma-facing surface	Heat flux of 10 and 20 MW/m^2
Bottom and side walls	Adiabatic
Symmetry plane	Symmetry
Heat sink	Robin BC

how with a 0.25–0.5 mm mesh it is possible to obtain fairly "grid-independent results", obtaining a grid convergence index on maximum temperatures in tungsten, copper and CuCrZr well below 1%.

The 2D thermal steady-state simulations are performed considering the Boundary Conditions (BCs) given in Table 3, while volumetric nuclear loads are neglected. Concerning the materials, temperature-dependent properties are considered for tungsten, CuCrZr and copper, respectively taken from [30–32].

Regarding the heat sink boundary, a Robin BC, necessary for the well-posedness of the problem, is assigned. A heat transfer coefficient is calculated based on the local CuCrZr temperature and the coolant pressure and bulk temperature, according to the procedure detailed in the following.

4.3.1. Heat transfer coefficient calculation

The correct calculation of the temperature distribution in the PFUs is possible only if a model capable of predicting the heat transfer coefficient for the part of the Nukiyama boiling curve of interest is available. The correlations adopted for the various heat transfer regimes are herewith reported.

Single-phase forced convection heat transfer

For the calculation of the single-phase convective heat transfer coefficient in turbulent flow regime, ADRANOS adopts the Sieder-Tate correlation [33] (valid for $Re > 10000$ and a broad range of Prandtl number Pr) with the Gambill correction factor [34] to take into account the presence of the ST (Eq. (14)).

$$Nu = 0.027 Re^{0.8} Pr\left(\overline{T},\overline{p}\right)^{1/3}\left(\frac{\mu_b\left(\overline{T},\overline{p}\right)}{\mu_w\left(T_w,\overline{p}\right)}\right)^{0.14}\left(2.18y^{-0.09}\right) \tag{14}$$

With reference to Eq. (14), Nu is the Nusselt number, Pr is calculated at the coolant average pressure and temperature, μ_w is the water dynamic viscosity calculated at the average coolant pressure and considering the local wall temperature T_w, while y is the ST twist ratio. From Eq. (14) is then possible to calculate the heat transfer coefficient and to evaluate the local heat flux q_{sp} according to Eq. (15), where λ is the fluid bulk thermal conductivity.

$$q_{sp} = \frac{Nu\lambda\left(\overline{T},\overline{p}\right)}{d_h}\left(T_w - \overline{T}\right) \tag{15}$$

Two-phase forced convection heat transfer

The correlations used for the various two-phase regimes of the Nukiyama boiling curve are taken entirely from [21,28].

Boiling incipience is evaluated by adopting the Bergles-Rohsenow correlation for the onset of nucleate boiling reported in Eq. (16), where the average pressure $\overline{p}$ is expressed in bar and q_{bi} is given in MW/m^2. The correlation is valid for water only, for a pressure range between 0.1 and 13.8 MPa [28].

$$q_{bi} = 1082\overline{p}^{1.156}\left(1.799\left(T_w - T_{sat}\right)\right)^{\frac{2.1598}{\overline{p}^{0.0234}}} \tag{16}$$

Fully developed nucleate boiling is evaluated with the Araki correlation, reported in Eq. (17) with $\overline{p}$ expressed in bar and q_{bi} in MW/m^2, while the partially developed nucleate boiling is calculated with the Bergles-Rohsenow correlation (Eq. (18)).

$$q_{fdnb} = 10^6\left(\frac{T_w - T_{sat}}{\left(25.72e^{\frac{-\overline{p}}{86}}\right)}\right)^3 \tag{17}$$

$$q_{pdnb} = \sqrt{q_{sp}^2 + \left(q_{fdnb} - q_{bi}\right)^2} \tag{18}$$

Although Araki's correlation is derived from experiments conducted with coolant inlet pressures up to 1.3 MPa and temperatures up to 80 °C, in [28] it is adopted up to significantly higher values of the two parameters, maintaining a very good agreement with the experimental data.

More in detail, according to the rationale defined in [35], the two-phase flow regime is calculated by adopting the partially developed nucleate boiling of Eq. (18). With this formulation, the heat flux asymptotically approaches fully developed boiling at high wall superheat. In particular, when the heat flux calculated with Eq. (15) is lower than the

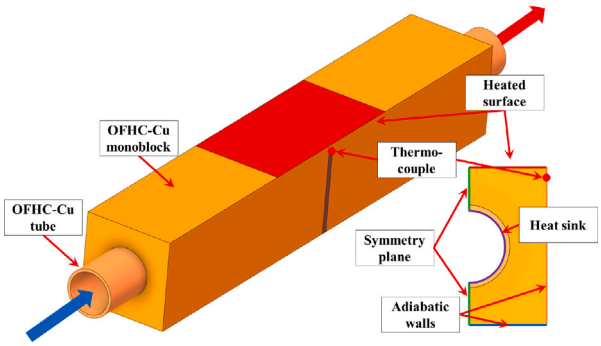

Fig. 11. Experimental setup adopted by Marshall and detail of the ADRANOS 2D domain.

one of Eq. (16), the formulation given in Eq. (15) is applied, otherwise, the heat flux is evaluated by adopting Eq. (18).

Finally, as regards the calculation of the CHF and the estimation of the post-CHF heat transfer regime (transition and film boiling), it should be noted that, according to the constraints discussed in Section 3, the divertor cooling circuit should allow operation with a CHF margin always higher than 1.4. Consequently, the post-CHF heat transfer coefficient calculation has not been currently implemented in ADRANOS, and the FEM module is executed uniquely when a CHF margin higher than 1 is obtained with the lumped-parameters module. When the CHF margin is lower than 1, instead, temperature values exceeding the pertaining limits are assigned on tungsten, copper, and CuCrZr.

Under single-phase and two-phase heat transfer conditions, an equivalent convective heat transfer coefficient is calculated, simply by dividing the heat flux by the temperature difference between the bulk of the fluid and the wall. Therefore, the Robin BC is assigned to the heat sink surface of Fig. 10 by providing both the coolant bulk temperature $\overline{T}$ and the equivalent heat transfer coefficient.

5. ADRANOS validation

To check the correctness of the implementation, ADRANOS underwent a validation campaign of both the FEM and the lumped-parameters modules. First, the experimental setup of [36] has been reproduced, and the outcomes of the stand-alone FEM module have been compared to the experimental data. Then, the divertor VTs cooling circuit of the DCC option has been studied with the aim to check if the results obtained under design operating conditions are in agreement with CFD calculations and if the temperature distributions in the monoblocks are in line with the results available in literature.

5.1. Marshall's experimental results validation case

The ADRANOS FEM module has been validated by comparing the code predictions with the experimental results obtained by Marshall [37] and reported in [38]. The comparison has been performed by reproducing Marshall's experimental setup reported in [36], by looking at the temperature of the Oxygen-Free High-Conductivity (OFHC) copper monoblock at the thermocouple location, i.e. 0.6 mm from the plasma-facing surface on the side of the monoblock, as shown in Fig. 11. The OFHC copper monoblock dimensions are 15.7 mm × 15.7 mm × 133.4 mm, while the length of the heated area (in red in Fig. 11) is 40 mm. The comparison between experimental and ADRANOS results is depicted in Fig. 12.

As can be seen, there is a very good correspondence between the ADRANOS results and the experimental data, with errors in predicting thermocouple temperatures within the ±10% range. At high heat flux values, a significant deviation between the curves is observed, related

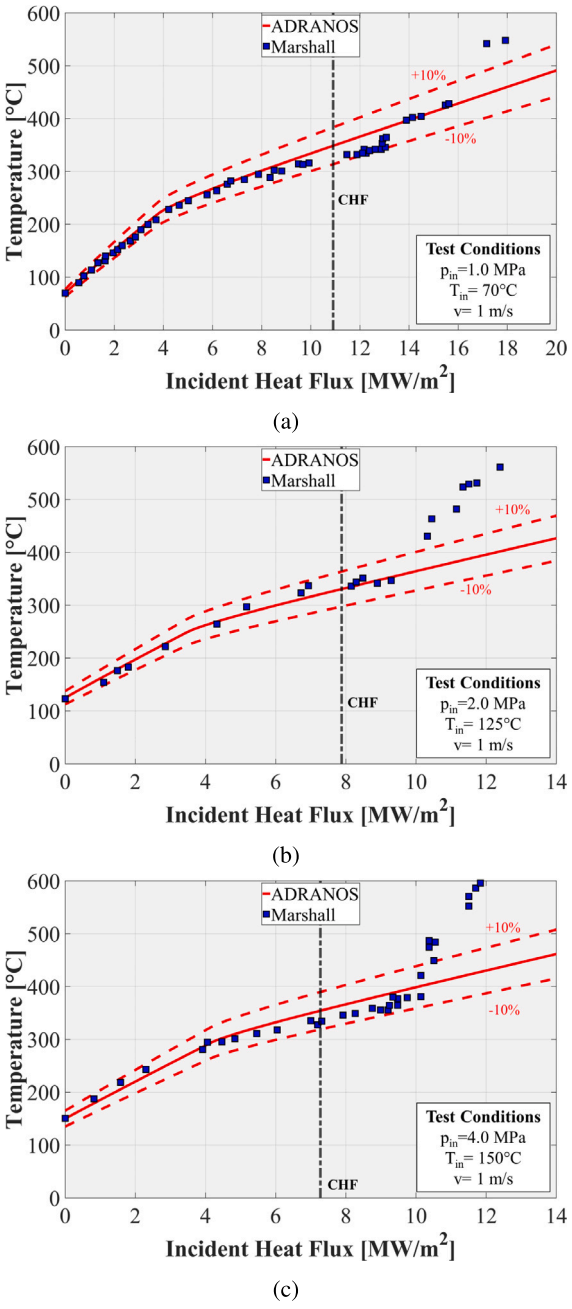

Fig. 12. Comparison between ADRANOS and Marshall's experimental results at inlet pressure of 1.0 (a), 2.0 (b) and 4.0 (c) MPa.

to the occurrence of the post-CHF heat transfer regime, not predicted by the calculation tool. However, this does not affect the predictive potential of the code since the divertor cooling circuit should never reach this boiling regime.

5.2. EU-DEMO divertor VTs cooling circuit validation case

The parametric study of the VTs cooling circuit (DCC option, 2019 design) has been carried out starting from the layout shown in Fig. 4 considering four different volumes: the IVT, the OVT, the inlet and the outlet manifolds.

The ADRANOS volumes have been defined considering integral surface and volumetric heat loads drawn from [9], while the pressure drop breakdown reported in [8] has been employed to define the

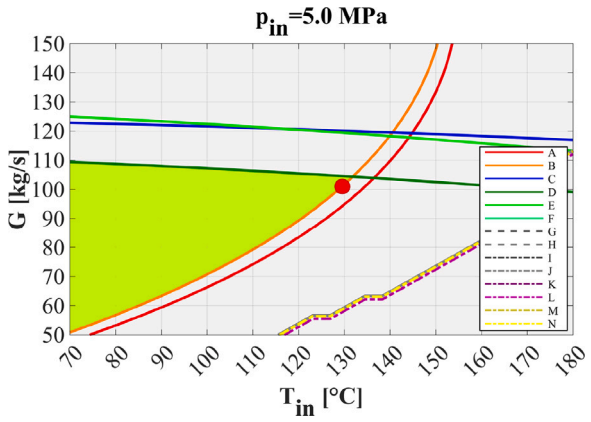

Fig. 13. Range of acceptable operating conditions for the VTs cooling circuit (DCC option, in green) and design operating point (in red).

Table 4
List of constraints and their IDs considered for the simulations.

ID	Constraint	Region	Load
A	$M_{CHF,min}$ = 1.4	OVT	20 MW/m^2
B	$M_{CHF,min}$ = 1.4	IVT	20 MW/m^2
C	Δp_{max} = 1.4 MPa	All	–
D	v_{max} = 16 m/s	OVT	–
E	v_{max} = 16 m/s	IVT	–
F	$\Delta T_{sat,min}$ = 20 °C	All	–
G	T_{max} = 300 °C	OVT CuCrZr	10 MW/m^2
H	T_{max} = 300 °C	IVT CuCrZr	10 MW/m^2
I	T_{max} = 450 °C	OVT CuCrZr	20 MW/m^2
J	T_{max} = 450 °C	IVT CuCrZr	20 MW/m^2
K	T_{max} = 3222 °C	OVT tungsten	20 MW/m^2
L	T_{max} = 3222 °C	IVT tungsten	20 MW/m^2
M	T_{max} = 885 °C	OVT Cu	20 MW/m^2
N	T_{max} = 885 °C	IVT Cu	20 MW/m^2

hydraulic characteristic functions. Since simulations of the VTs cooling circuit at different mass flow rates are not available, a value of 2 has been selected for the γ exponent of Eq. (1).

The analysis has been carried out by keeping the coolant inlet pressure fixed at 5.0 MPa while varying both the inlet temperature and the total mass flow rate, respectively from 70 to 180 °C and from 50 to 150 kg/s. The selected inlet temperature and mass flow rate ranges have been discretized with 30 points each, for a total of 900 cases. The overall run time to perform all the simulations was of approximately 13 min on a 3.00 GHz 18 core i9-9980XE workstation.

The results obtained are shown in Fig. 13, with reference to the constraints listed in Table 4. The figure shows the region in which the circuit can operate in compliance with all the selected constraints (filled in green) and indicates in red the VTs cooling circuit design operating point, i.e. G = 98.6 kg/s and T_{in} = 130 °C.

Fig. 13 shows that the design operating point is close to the intersection of two constraint curves: the CHF margin at the IVT (curve B) and the maximum coolant velocity in the OVT (curve D). These same curves entirely delimit the green region in the figure, while all other constraints are less relevant, including the temperatures in the PFUs.

A comparison between the results obtained by ADRANOS for the design operating point with those of the 3D-CFD analysis of [8] is reported in Table 5. As it may be argued from the table, there is a very good prediction of the overall pressure drop, of the axial fluid velocities that occur in the targets, and of the CHF margins, with relative errors below 3%. Furthermore, the results obtained with ADRANOS are conservative if compared to those of the detailed CFD calculations, as the coolant velocities and the CHF margins are closer to the limit values reported in Table 4. These findings are not surprising since the ADRANOS simulation has been set on the basis of the results of the 3D-CFD analysis.

Table 5
Comparison between ADRANOS and CFD results.

	CFD	ADRANOS
Δp_{tot} [MPa]	0.94	0.94
v_{OVT} [m/s]	14.91	15.09
v_{IVT} [m/s]	13.18	13.22
$M_{CHF,OVT}$ [–]	1.49	1.43
$M_{CHF,IVT}$ [–]	1.41	1.38

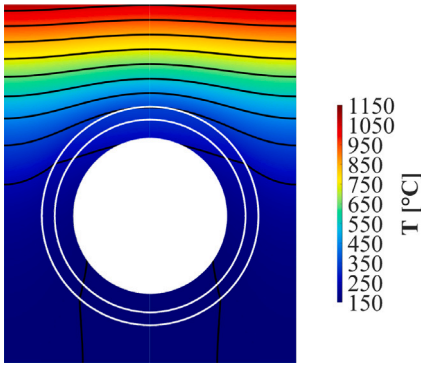

Fig. 14. Temperature distributions for an OVT PFU under an incident heat flux of 10 MW/m^2.

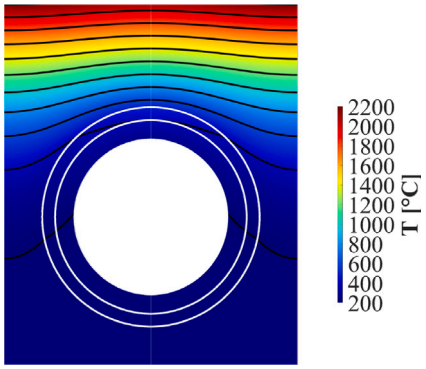

Fig. 15. Temperature distributions for an OVT PFU under an incident heat flux of 20 MW/m^2.

To further validate the ADRANOS FEM module, the thermal field within the monoblocks has been evaluated under design operating conditions. In particular, Fig. 14 shows the thermal field predicted by the code for an OVT PFU considering an incident heat flux of 10 MW/m^2. Under these load conditions, the maximum temperature predicted in tungsten is around 1100 °C, in good agreement with the value reported in [2]. Considering instead an incident heat flux of 20 MW/m^2, the temperature distribution depicted in Fig. 15 is obtained, with a maximum tungsten temperature of approximately 2220 °C. Similar temperature fields are obtained for the IVT PFU, as the slightly different local coolant conditions do not affect significantly the results of the FEM analyses.

Further tests, not reported here for the sake of brevity, have been carried out considering the PFUs with a height of 25 mm (and not 28 mm as in the reference case, so decreasing the thickness of tungsten in the plasma-facing region of 3 mm). In this case, the predicted maximum temperature value in tungsten is approximately 830 °C under an incident heat flux of 10 MW/m^2. This maximum temperature is in good agreement with the results presented in [39] for the same monoblock geometry, with a relative error of ≈6%.

Table 6
Deposited volumetric and surface power breakdown for each SCC option divertor cassette.

Component	Power [MW]	
	Volumetric	Surface
CB	0.717	–
SL	1.558	0.771
RPs	0.150	0.062
NSs	0.030	–
IVT	0.620	1.045
OVT	0.633	1.385
TOTAL	**3.707**	**3.263**

6. Application of ADRANOS to the EU-DEMO divertor SCC option cooling circuit

In this section, ADRANOS is employed to study the performance map of the EU-DEMO divertor SCC option, starting from the 2021 cooling circuit design described in Section 2.2 and considering three additional cases. The study has been carried out with the aim of exploring if it is possible to increase the coolant inlet temperature (to improve the divertor lifetime) by selecting optimal operating conditions, adopting different cooling circuit layouts, or optimizing the circuit to reduce pressure losses.

6.1. 2021 Design cooling circuit

The parametric study of the EU-DEMO divertor SCC option has been carried out starting from the cooling circuit breakdown shown in Fig. 8, referring to the results reported in [40] for the hydraulic characterization. Since CFD results are not available at different values of coolant mass flow rate, the exponent γ of the characteristic function has been set to 2 for all the volumes. Regarding thermal loads, the values reported in Table 6 have been adopted, where the volumetric loads have been drawn from dedicated neutronic analyses of the 2021 divertor design [41] and the surface loads from [6].

The analysis has been performed considering a coolant inlet pressure of 5.0, 7.5, 10.0, and 15.0 MPa, varying the overall flow rate from 20 to 60 kg/s and the inlet temperature from 70 to 180 °C. The selected inlet temperature and mass flow rate ranges have been discretized with 30 points each, for a total of 3600 cases, while the overall run time to perform all the simulations was approximately 1 h and 18 min on a 3.00 GHz 18 core i9-9980XE workstation.

The results obtained are shown in Fig. 16, with reference to the constraints listed in Table 4. Several considerations can be derived:

- the green region is limited only by the pressure drop (curve C) and the CHF margin of the OVT (curve A) at 5.0 and 7.5 MPa;
- at higher pressures (≥10.0 MPa), the constraint on maximum OVT CuCrZr temperature at 10 MW/m^2 comes into play (curve G). This constraint completely delimits the green area together with the pressure drop curve at 15.0 MPa;
- the OVT is the critical component in terms of CHF margin and monoblock temperature. The reason is that the two targets are connected in series and the same mass flow rate is distributed among a greater number of PFUs within the OVT, resulting in lower coolant velocities and thus lower CHF margins and heat transfer coefficients, resulting in higher structure temperatures;
- curve G set a maximum coolant inlet temperature of ≈154 °C (Fig. 16(d)) which cannot be increased by further raising the coolant pressure. In fact, single-phase heat transfer conditions are observed at 10 MW/m^2 and the heat transfer coefficient calculated for this heat transfer regime is marginally affected by coolant pressure;

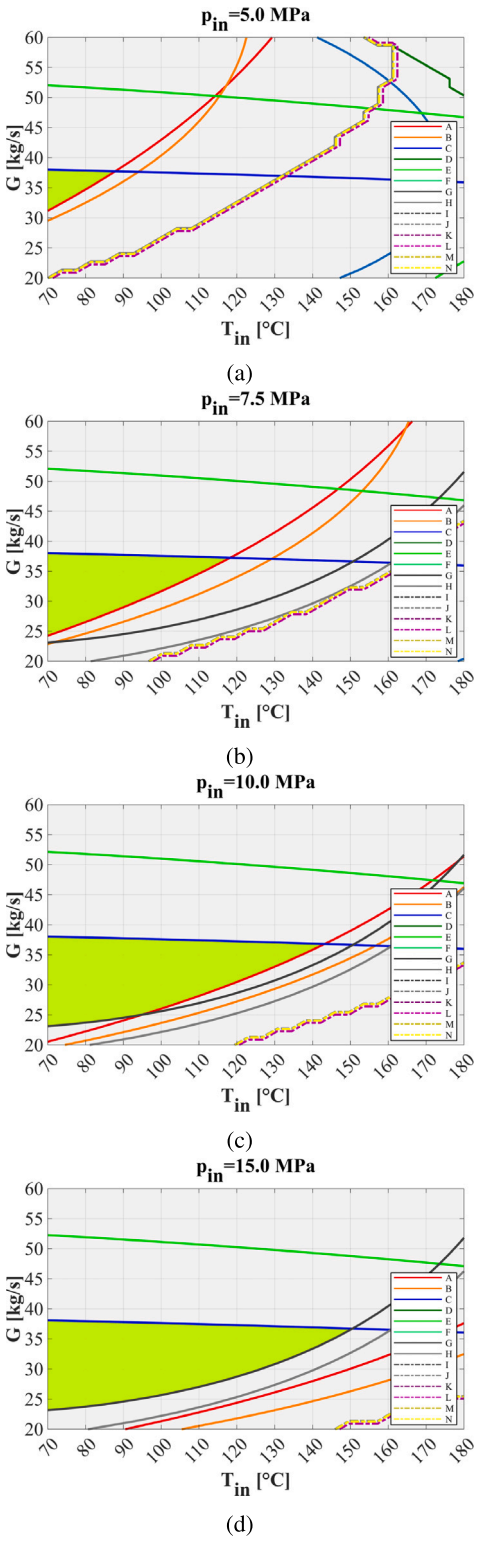

Fig. 16. Range of acceptable operating conditions for the SCC option divertor (in green) for an inlet pressure of 5.0 (a), 7.5 (b), 10.0 (c), and 15.0 (d) MPa.

- the current divertor cassette is designed to withstand a pressure of 5.0 MPa. Therefore, the results obtained at higher coolant pressures should be considered as qualitative, as a thorough revision of the cassette design should be required to guarantee its structural integrity;

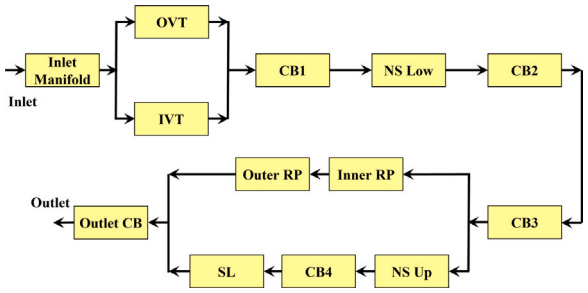

Fig. 17. Flowchart of the EU-DEMO divertor SCC option with VTs in parallel.

- at a coolant inlet pressure of 5.0 and 7.5 MPa, the 2021 design SCC divertor can operate with maximum inlet coolant temperatures of respectively 85 and 115 °C. Under these conditions, a component lifetime of ≈0.8 and ≈0.9 fpy can be respectively estimated using the same reasoning on the maximum irradiation dose damage as in [17], well below the requirement on divertor lifetime.

6.2. Optimized 2021 design cooling circuit

The first additional case investigates how the results are affected if the total pressure drop of the cooling circuit is drastically reduced. This cooling circuit optimization is highly unlikely, as most of the pressure losses occur in the components directly exposed to the plasma (VTs, SL and RPs). These components are equipped with small cooling channels and high coolant velocities are required to provide the necessary cooling of the structures, thus definitely resulting in high pressure losses.

However, even considering this case, the maximum coolant operating temperature can only be increased to a small extent. In fact, looking at Fig. 16, the acceptable operating region of the circuit would be delimited by the OVT CHF margin curve and the maximum velocity in the IVT PFU channels (curve E) in the absence of the pressure drop constraint. Consequently, it would be possible to reach up to ≈115 °C coolant inlet temperature at an inlet pressure of 5.0 MPa, and up to ≈145 °C at 7.5 MPa.

More realistically, an optimization of the hydraulic circuit could allow an increase in operating temperature of only a few degrees, not solving the issues related to the component lifetime.

6.3. VTs in parallel

The second additional case studied is the adoption of a parallel connection between the two VTs, similarly to the DCC divertor option VTs cooling circuit. The flowchart adopted for this analysis is shown in Fig. 17, while loads, coefficients of the characteristic functions and assumptions are the same as those used for the baseline cooling circuit. The results obtained are depicted in Fig. 18.

Considering an inlet coolant pressure of 5.0 MPa, no acceptable operating condition can be found. At higher coolant inlet pressure values, the SCC option with VTs in parallel allows operation only at lower coolant temperatures with respect to the configuration with targets in series. Additionally, by increasing the inlet pressure of the coolant up to 15.0 MPa, it is possible to increase the inlet temperature up to a maximum of ≈115 °C due to the constraints on CuCrZr temperature.

6.4. VTs in parallel and CB bypass

Lastly, a case with VTs connected in parallel and a bypass line connecting the outlet of the targets to the outlet of the cassette has been considered. This line ensures that only part of the coolant mass flow rate is fed to the CB while maintaining the full flow rate at the VTs. With this cooling circuit layout is possible to increase the mass flow rate fed to the circuit while avoiding unduly high pressure losses. If the same solution is applied to the series-connected VTs, the results are equivalent to those of the cooling circuit optimization case.

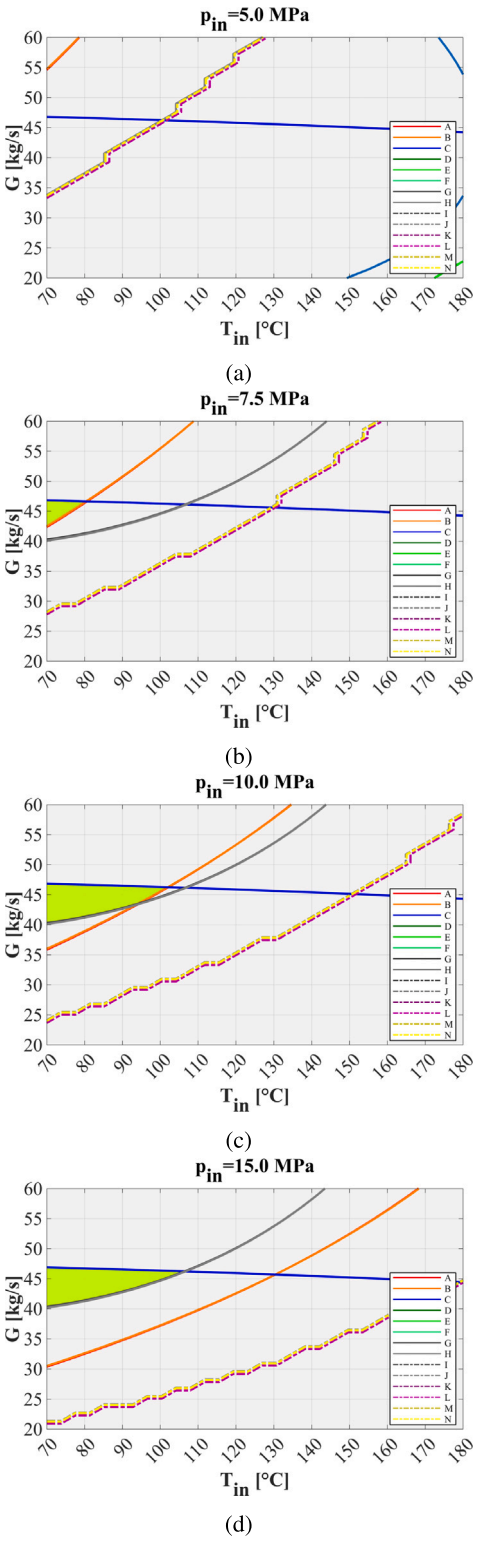

Fig. 18. Range of acceptable operating conditions for the SCC option divertor with VTs in parallel (in green) for an inlet pressure of 5.0 (a), 7.5 (b), 10.0 (c), and 15.0 (d) MPa.

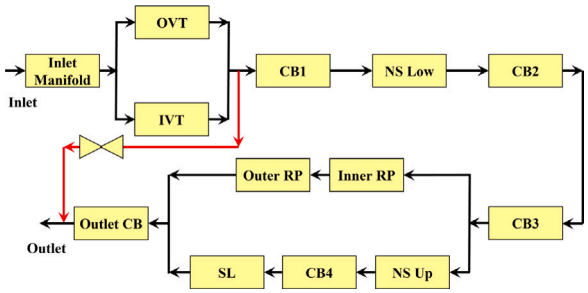

Fig. 19. Flowchart of the EU-DEMO divertor SCC cooling option with VTs in parallel and CB bypass.

Reference is made to the flowchart shown in Fig. 19, where the bypass line is shown in red. The bypass line has been modelled by imposing a fixed mass flow rate through the CB equal to 35 kg/s for all the operating conditions of the map. This mass flow rate value is close to the one adopted for the DCC option divertor CB [42], so it can surely provide adequate cooling to the components.

In addition, with reference to Fig. 19, the value of the characteristic function coefficient α (see Eq. (1)) of the Inlet Manifold volume has been reduced by a factor of 10. This reduction is necessary to avoid excessively high pressure drops inside the Inlet Manifold, which has been originally designed to route a significantly lower mass flow rate.

The results obtained are reported in Fig. 20. As can be seen, the green region is delimited here by the CHF margin curves in the lower part and by the maximum coolant velocity curves in the upper part. Moreover, the green region is delimited by the CuCrZr temperature constraint in the lower part at high coolant pressure values. Comparing the results shown here with those of the previous sections, the gain obtained with the CB bypass is remarkable, with a maximum value of coolant inlet temperature of ≈135 °C at 5.0 MPa, 175 °C at 7.5 MPa, and 195 °C at 15.0 MPa.

Although this configuration appears promising, some additional issues should be considered: it is necessary to adopt properly sized orifices downstream of the targets, capable of producing a localized pressure loss of ≈0.7 MPa in the bypass line, resulting in high localized coolant velocities that could cause erosion problems. Moreover, considering the coolant operating point at the maximum allowable coolant inlet temperature of Fig. 20(d), the orifice alone would result in a loss of fluid mechanical power in the order of ≈60 kW per cassette (approximately equal to the 50% of the pumping power required by both the CB and VTs cooling circuit of the DCC option [2]), which would have to be supplied to the fluid by the circulation pumps. Finally, it should be further investigated the behaviour of the cooling circuit under transient conditions, and the possibility to establish flow distribution instabilities between the CB and the bypass line, which could potentially pose a risk to the structural integrity of the cassette.

6.5. Summary and discussion on EU-DEMO divertor SCC results

The results obtained considering the EU-DEMO divertor SCC option 2021 design and the three additional cases discussed above are summarized in Table 7.

As can be observed from the table, the most promising SCC option divertor arrangement is the one with targets in parallel and CB bypass. By adopting this configuration, the coolant inlet temperature, and thus the lifetime of the divertor cassette, can be comparable with the one of the baseline DCC option but, as discussed in Section 3, it will not meet in any case the divertor lifetime requirement. Moreover, also accepting this result, this cooling circuit layout would entail the criticalities discussed in the previous section, making it doubtful whether this solution may be adopted.

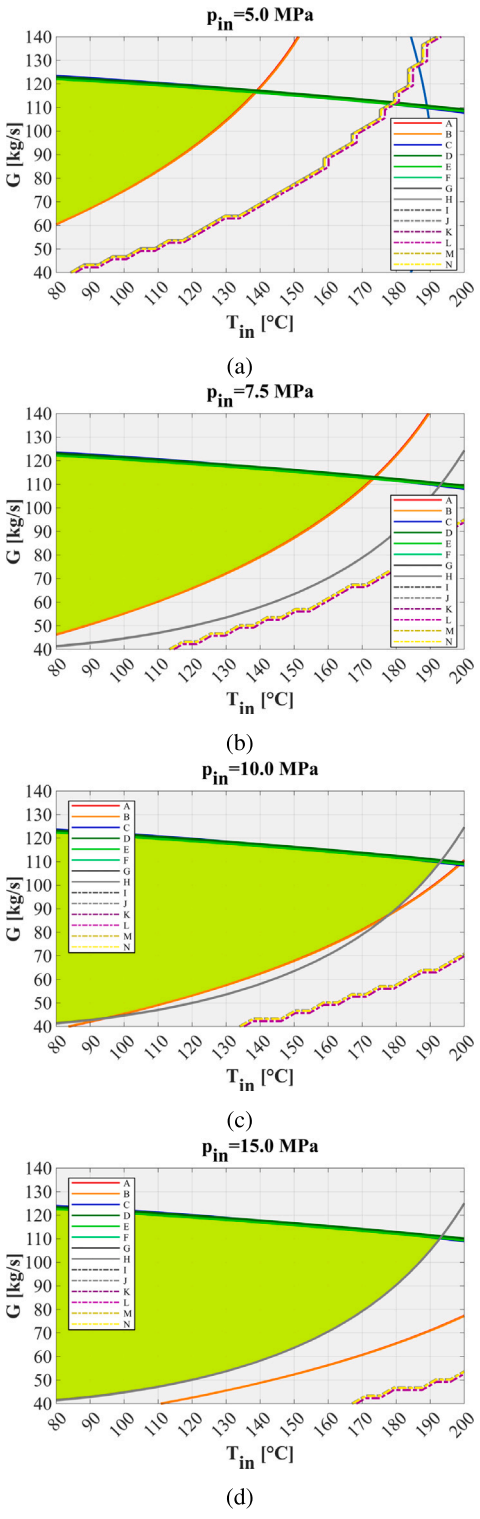

Fig. 20. Range of acceptable operating conditions for the SCC option divertor with VTs in parallel and CB bypass (in green) for an inlet pressure of 5.0 (a), 7.5 (b), 10.0 (c), and 15.0 (d) MPa.

With other cooling circuit layouts and adopting coolant inlet pressure values up to 7.5 MPa, it is realistically not possible to exceed a maximum coolant inlet temperature of ≈120 °C, regardless of the VTs arrangement, definitely resulting in a cassette lifetime lower than 1 fpy. At higher pressures, it is possible to increase these values, but, as can be argued from the summary, it is not feasible to obtain the same

Table 7
Summary of the maximum coolant inlet temperature values obtained for the different EU-DEMO divertor SCC option cooling circuit cases.

Scenario	p_{in}		
	5.0 MPa	7.5 MPa	15.0 MPa
2021 SCC design	≈85 °C	≈115 °C	≈155 °C
SCC optimization	<115 °C	<145 °C	<175 °C
Par. VTs	–	≈80 °C	≈115 °C
Par. VTs and Bypass	≈135 °C	≈175 °C	≈195 °C

inlet temperature of the CB circuit as in the DCC configuration, which would lead to a divertor lifetime lower than 1.2 fpy. Furthermore, it would be necessary to significantly change the divertor design in order to withstand the mechanical loads deriving from the increased coolant pressure.

7. Conclusions

In the framework of the activities of the EUROfusion action, UNIPA carried out a research campaign to study the new EU-DEMO divertor SCC option, which foresees the integration of the VTs and the CB cooling circuits.

To find suitable operating conditions able to fulfil the different thermal and thermal-hydraulic constraints and requirements of the divertor, the UNIPA thermal-hydraulic research unit has developed ADRANOS, a coupled lumped-parameter/2D-FEM code able to quickly determine the operating map of the divertor cooling circuit. ADRANOS has been properly validated against experimental data, CFD and thermal calculations, and has been used to study the SCC option divertor 2021 design and three additional cases. The analyses highlighted the criticalities of adopting the SCC option for EU-DEMO, as CHF margin and pressure drop requirements allow for operation only at low coolant temperatures, limiting the divertor lifetime if Eurofer is employed as structural material. Moreover, the analyses reported here pointed out how it is not possible to significantly increase the divertor lifetime by acting on the coolant pressure, as the constraints on monoblock temperature pose an upper bound on the coolant temperature. Furthermore, even considering an optimized cooling circuit with reduced losses or the adoption of a complex layout with a CB bypass line, the maximum coolant inlet temperature is still limited by the maximum PFU coolant velocity. As a result, the divertor lifetime obtained is always lower than the 1.5 fpy requirement for all the cases investigated.

The outcomes presented here are the result of the actual assumptions in terms of plasma surface heat load, the current design and technology of the VTs, as well as the still incomplete knowledge of the properties of the adopted materials exposed to high levels of neutron-induced damage at low operating temperatures. Additionally, a different rationale for the calculation of the divertor lifetime based on less conservative criteria, as suggested in [2], would probably result in a longer lifetime for the divertor. However, under the assumptions and requirements currently adopted for the EU-DEMO divertor and considering the cases presented here, the SCC option divertor would certainly simplify the design of the balance of plant and the cassette maintenance operations, but it is doubtful whether it is compatible with the adoption of Eurofer as structural material, as it is not possible to guarantee the desired component lifetime.

CRediT authorship contribution statement

A. Quartararo: Conceptualization, Methodology, Investigation, Writing – original draft. **P.A. Di Maio:** Conceptualization, Methodology, Investigation, Writing – original draft. **E. Vallone:** Conceptualization, Methodology, Investigation, Writing – original draft.

Declaration of competing interest

The authors declare that they have no known competing financial interests or personal relationships that could have appeared to influence the work reported in this paper.

Data availability

Data will be made available on request.

Acknowledgements

This work has been carried out within the framework of the EUROfusion Consortium, funded by the European Union via the Euratom Research and Training Programme (Grant Agreement No 101052200 — EUROfusion). Views and opinions expressed are however those of the author(s) only and do not necessarily reflect those of the European Union or the European Commission. Neither the European Union nor the European Commission can be held responsible for them.

References

[1] T. Donné, W. Morris, European Research Roadmap to the Realisation of Fusion Energy, 2018, ISBN: 978-3-00-061152-0.
[2] J.H. You, et al., Divertor of the European DEMO: Engineering and technologies for power exhaust, Fusion Eng. Des. 175 (2022) 113010, http://dx.doi.org/10.1016/j.fusengdes.2022.113010.
[3] G. Federici, W. Biel, M.R. Gilbert, R. Kemp, N. Taylor, R. Wenninger, European DEMO design strategy and consequences for materials, Nucl. Fusion 57 (9) (2017) 092002, http://dx.doi.org/10.1088/1741-4326/57/9/092002.
[4] U. Bonavolontà, et al., EU-DEMO divertor: Cassette design and PFCs integration at pre-conceptual stage, Fusion Eng. Des. 159 (2020) http://dx.doi.org/10.1016/j.fusengdes.2020.111784.
[5] G. Federici, et al., Overview of the DEMO staged design approach in europe, Nucl. Fusion 59 (6) (2019) 066013, http://dx.doi.org/10.1088/1741-4326/ab1178.
[6] A. Quartararo, et al., Thermofluid-dynamic assessment of the EU-DEMO divertor single-circuit cooling option, Fusion Eng. Des. 188 (2023) 113408, http://dx.doi.org/10.1016/j.fusengdes.2022.113408.
[7] J.H. You, et al., Conceptual design studies for the European DEMO divertor: Rationale and first results, Fusion Eng. Des. 109–111 (2016) 1598–1603, http://dx.doi.org/10.1016/j.fusengdes.2015.11.012.
[8] P.A. Di Maio, et al., Hydraulic assessment of an upgraded pipework arrangement for the DEMO divertor plasma facing components cooling circuit, Fusion Eng. Des. 168 (2021) 112368, http://dx.doi.org/10.1016/j.fusengdes.2021.112368.
[9] G. Mazzone, et al., Eurofusion-DEMO divertor - cassette design and integration, Fusion Eng. Des. 157 (2020) 111656, http://dx.doi.org/10.1016/j.fusengdes.2020.111656.
[10] D. Marzullo, et al., DIV-JUS-2-CD1 Divertor System Detailed Design Description, 2020, EUROfusion IDM Ref.: 2NSLJP.
[11] P.A. Di Maio, G. Mazzone, A. Quartararo, E. Vallone, J.H. You, Thermal-hydraulic study of the DEMO divertor cassette body cooling circuit equipped with a liner and two reflector plates, Fusion Eng. Des. 167 (2021) 112227, http://dx.doi.org/10.1016/j.fusengdes.2021.112227.
[12] D. Marzullo, et al., DEMO_DIVERTOR_2021_single_cooling, 2022, EUROfusion IDM Ref.: 2PRJTE.
[13] A.R. Raffray, et al., Critical heat flux analysis and R&D for the design of the ITER divertor, Fusion Eng. Des. 45 (4) (1999) 377–407, http://dx.doi.org/10.1016/S0920-3796(99)00053-8.
[14] P.A. Di Maio, et al., On the numerical assessment of the thermal-hydraulic operating map of the DEMO divertor plasma facing components cooling circuit, Fusion Eng. Des. 161 (2020) 111919, http://dx.doi.org/10.1016/j.fusengdes.2020.111919.
[15] F. Maviglia, et al., Impact of plasma-wall interaction and exhaust on the EU-DEMO design, Nucl. Mater. Energy 26 (2021) 100897, http://dx.doi.org/10.1016/j.nme.2020.100897.
[16] F. Domptail, T.R. Barrett, M. Fursdon, A. Lukenskas, J.H. You, The design and optimisation of a monoblock divertor target for demo using thermal break interlayer, Fusion Eng. Des. 154 (2020) 111497, http://dx.doi.org/10.1016/j.fusengdes.2020.111497.
[17] G. Mazzone, et al., Choice of a low operating temperature for the DEMO EUROFER97 divertor cassette, Fusion Eng. Des. 124 (2017) 655–658, http://dx.doi.org/10.1016/j.fusengdes.2017.02.013.
[18] The MathWorks, Inc., MATLAB Primer, 2021, Release: R2021b.
[19] Featool multiphysics v1.15, user's guide, 2021, URL https://www.featool.com.

[20] A.R. Raffray, G. Federici, RACLETTE: a model for evaluating the thermal response of plasma facing components to slow high power plasma transients. Part I: Theory and description of model capabilities, J. Nucl. Mater. 244 (2) (1997) 85–100, http://dx.doi.org/10.1016/S0022-3115(96)00680-0.

[21] T.D. Marshall, D.L. Youchison, L.C. Cadwallader, Modeling the nukiyama curve for water-cooled fusion divertor channels, Fusion Technol. 39 (2P2) (2001) 849–855, http://dx.doi.org/10.13182/FST01-A11963345.

[22] Z.J. Jackson, J.R. Nicholas, P.T. Ireland, Development of a 1D thermofluid code for divertor target plate modeling, Fusion Eng. Des. 147 (2019) 111237, http://dx.doi.org/10.1016/j.fusengdes.2019.06.010.

[23] S.E.-D. El-Morshedy, Thermal-hydraulic modelling and analysis of ITER tungsten divertor monoblock, Nucl. Mater. Energy 28 (2021) 101035, http://dx.doi.org/10.1016/j.nme.2021.101035.

[24] M. Holmgren, X steam, thermodynamic properties of water and steam, 2022, MATLAB Central File Exchange. Retrieved March, 2022.

[25] International Association for the Properties of Water and Steam, Revised Release on the IAPWS Industrial Formulation 1997 for the Thermodynamic Properties of Water and Steam, 2007.

[26] J. Kiefer, Sequential minimax search for a maximum, Proc. Amer. Math. Soc. 4 (3) (1953) 502–506.

[27] F. Inasaka, H. Nariai, Evaluation of subcooled critical heat flux correlations for tubes with and without internal twisted tapes, Nucl. Eng. Des. 163 (1) (1996) 225–239, http://dx.doi.org/10.1016/0029-5493(95)01170-6.

[28] Sandia National Laboratories and United States. Department of Energy. Office of Scientific and Technical Information, FILM-30: A Heat Transfer Properties Code for Water Coolant, United States. Department of Energy, 2001.

[29] L. Eça, M. Hoekstra, A procedure for the estimation of the numerical uncertainty of cfd calculations based on grid refinement studies, J. Comput. Phys. 262 (2014) 104–130, http://dx.doi.org/10.1016/j.jcp.2014.01.006.

[30] E. Gaganidze, et al., DEMO-DEF-1-CD1 - Materials Properties Handbook - Tungsten, 2020, EUROfusion IDM Ref.: 2P3SPL.

[31] E. Gaganidze, et al., DEMO-DEF-1-CD1 - Materials Properties Handbook - CuCrZr, 2020, EUROfusion IDM Ref.: 2NV3Q6.

[32] Y.S. Touloukian, R.W. Powell, C.Y. Ho, P.G. Klemens, Thermophysical Properties of Matter - The TPRC Data Series. Volume 1. Thermal Conductivity - Metallic Elements and Alloys, Tech. rep., Thermophysical and Electronic Properties Information Analysis Center Lafayette, IN, 1970.

[33] T.L. Bergman, A.S. Lavine, F.P. Incropera, D.P. DeWitt, Fundamentals of Heat and Mass Transfer, 8th Edition, Wiley, 2017.

[34] W.R. Gambill, Heat Transfer, Burnout, and Pressure Drop for Water in Swirl Flow Through Tubes with Internal Twisted Tapes, vol. 2911, Oak Ridge National Laboratory, 1960.

[35] A.E. Bergles, W.M. Rohsenow, The determination of forced-convection surface-boiling heat transfer, J. Heat Transfer 86 (3) (1964) 365–372, http://dx.doi.org/10.1115/1.3688697.

[36] T.D. Marshall, J.M. McDonald, L.C. Cadwallader, D. Steiner, An experimental examination of the loss-of-flow accident phenomenon for prototypical ITER divertor channels of y=0 and y=2, Fusion Technol. 37 (1) (2000) 38–53, http://dx.doi.org/10.13182/FST00-A120.

[37] T.D. Marshall, Experimental Examination of the Postcritical Heat Flux and Loss-of-Flow Accident Phenomena for Prototypical ITER Divertor Channels, Rensselaer Polytechnic Institute, 1999.

[38] S.E.-D. El-Morshedy, A. Hassanein, Transient thermal hydraulic modeling and analysis of ITER divertor plate system, Fusion Eng. Des. 84 (12) (2009) 2158–2166, http://dx.doi.org/10.1016/j.fusengdes.2009.02.051.

[39] F. Crescenzi, H. Greuner, S. Roccella, E. Visca, J.H. You, ITER-like divertor target for DEMO: Design study and fabrication test, Fusion Eng. Des. 124 (2017) 432–436, http://dx.doi.org/10.1016/j.fusengdes.2017.02.014.

[40] P.A. Di Maio, et al., Divertor Thermo-Hydraulic Assessment 2021, Deliverable DIV-DEMO.S.1-T002-D001, 2022, EUROfusion IDM Ref.: 2PHWSW.

[41] R. Villari, et al., DIV-DEMO.S.1-T003-D001-Neutronics Villari, 2021, EUROfusion IDM Ref.: 2NKBSA.

[42] P.A. Di Maio, et al., On the thermal-hydraulic performances of the DEMO divertor cassette body cooling circuit equipped with a liner, Fusion Eng. Des. 156 (2020) 111613, http://dx.doi.org/10.1016/j.fusengdes.2020.111613.